Available online at www.sciencedirect.com
SCIENCE DIRECT®
Physica D 209 (2005) 135–144
PHYSICA D
www.elsevier.com/locate/physd

On nontrivial traveling waves in thin film flows including contact lines

Lou Kondic[a,*], Javier A. Diez[b,1]

[a] *Department of Mathematical Sciences, Center for Applied Mathematics and Statistics, New Jersey Institute of Technology, Newark, NJ 07102, USA*
[b] *Instituto de Física Arroyo Seco, Universidad Nacional del Centro de la Provincia de Buenos Aires, Pinto 399, 7000 Tandil, Argentina*

Available online 20 July 2005

Abstract

We discuss dynamics of thin liquid films spreading down an inclined plane. The fronts of these films are known to be unstable with respect to formation of finger-like and triangular patterns. In this work, we concentrate on one particular aspect of these flows, and that is the existence of nonlinear traveling waves. We find evidence for presence of these waves for all inclination angles less than 90°. To understand better the relevant pattern formation mechanism, we explore via numerical simulations the bifurcation structure of the stability diagram close to the critical wavenumber. The recovered structure is consistent with the existence of a subcritical bifurcation. We discuss the connection between the bifurcation diagram and the existence of nontrivial traveling waves.

Keywords: Liquid thin films; Contact line; Bifurcations

1. Introduction

Flow of thin liquid films is a well studied problem, motivated both by numerous applications [1], and by some very interesting mathematical questions. These flows can involve a number of different effects, including non-Newtonian fluid behavior [2,3], partial wetting and related dewetting effects [4–6], flow on heterogeneous surfaces [7,8], spreading of surfactants [9], or spreading under competing thermal and body forces leading to undercompressive shocks [10]. An aspect of the flow of thin films which is of particular interest to us is the instability of the fluid front as it flows under gravity down an incline. This problem has also been considered by a number of researchers, e.g. [11–15]. This instability is known to lead to formation of patterns which could be of either finger-like or triangular shape. Our earlier works have shown that the shape of these patterns is governed by the inclination angle, or, more generally, by the relative strength of two gravity terms – convective term that drives the flow (and

[1] Researcher of CONICET, Argentina.
* Corresponding author.
E-mail addresses: kondic@njit.edu (L. Kondic), jdiez@exa.unicen.edu.ar (J.A. Diez).

0167-2789/$ – see front matter © 2005 Elsevier B.V. All rights reserved.
doi:10.1016/j.physd.2005.06.029

instability), and hydrostatic pressure term that plays a stabilizing role [16,17].

In this work we concentrate on the particular problem of the manner in which the patterns grow in the gravity driven flow of completely wetting fluids. In addition, we concentrate the discussion on the constant flux flow, where the thickness of the fluid far behind the front is fixed to a constant value. We discuss whether the resulting patterns grow for all times, or whether growth saturation (i.e., finite pattern length) is expected. This issue is of relevance to a number of applications of thin film flows, driven either by gravity or by other forces of mechanical (e.g. centrifugal), chemical, or thermal (e.g. Marangoni forces) origin. In addition, we expect that understanding this problem will also shed some light on still not completely resolved issue of instability for very small inclination angles and related transient growth effects [13,18–20]. We note that some earlier results regarding the growth saturation have been presented in [17]. Here we extend these results by analyzing more precisely the instability development close to the bifurcation point of the governing equation.

2. Formulation of the problem

Dynamics of thin liquid films is typically analyzed within the framework of lubrication approximation. The assumptions of this approach, as well as the details of our computational methods are given elsewhere; see [21] and the references therein. For completeness, here we give a basic outline, concentrating on the aspects relevant to the main subject of this work.

Fig. 1 shows the basic geometry of the flow with well known capillary ridge forming behind the advancing contact line (contact point in two space dimensions). Within the lubrication approximation, one uses the fact that the film thickness is much smaller than any in-plane $(x - y)$ dimension. After depth-averaging the fluid velocity over short (z) direction, and using no-slip boundary condition at the solid–liquid interface, the continuity equation yields the following equation for the height, h, of the (incompressible) liquid film:

$$\frac{\partial h}{\partial t} = -\frac{1}{3\mu}\nabla\cdot[\gamma h^3\nabla\nabla^2 h - \rho g h^3\nabla h\,\cos\alpha + \rho g h^3\,\sin\alpha\,\mathbf{i}], \tag{1}$$

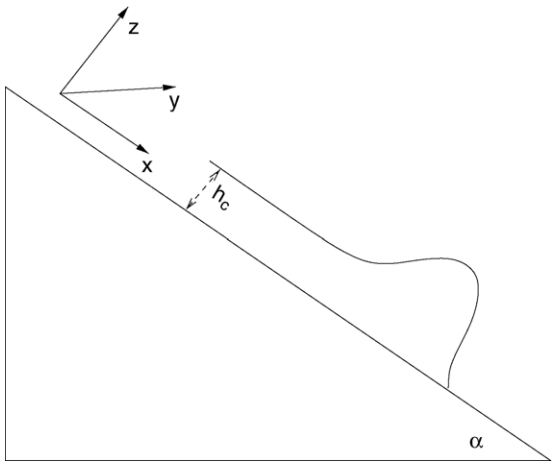

Fig. 1. Sketch of the flow geometry before the onset of instability.

where $\nabla = (\partial_x, \partial_y)$, x points down the incline, and y is in the transverse direction. Here, $\mu, \rho, g, \gamma, \alpha$ are the viscosity, density, gravity, surface tension, and the inclination angle, respectively. The fourth order term results from surface tension, and the last two terms are due to gravity.

To balance viscous and capillary forces in Eq. (1), we scale h by the fluid thickness far behind the contact line, h_c, and define the scaled in-plane coordinates and time by $(\bar{x}, \bar{y}, \bar{t}) = (x/x_c, y/x_c, t/t_c)$, where

$$x_c = \left(\frac{a^2 h_c}{\sin\alpha}\right)^{1/3}, \qquad t_c = \frac{3\mu}{\gamma}\frac{a^2 x_c}{h_c^2\,\sin\alpha} \tag{2}$$

and $a = \sqrt{\gamma/\rho g}$ is the capillary length. The velocity scale is chosen naturally as $U = x_c/t_c$, and the capillary number is defined as $Ca = \mu U/\gamma$. Using this nondimensionalization, Eq. (1) for $h = h/h_c$ is given by (dropping the bars)

$$\frac{\partial h}{\partial t} + \nabla\cdot[h^3\nabla\nabla^2 h] - D(\alpha)\nabla\cdot[h^3\nabla h] + \frac{\partial h^3}{\partial x} = 0, \tag{3}$$

where the single dimensionless parameter $D(\alpha) = (3Ca)^{1/3}\cot(\alpha)$ measures the size of the normal component of gravity.

All theoretical and computational methods require some regularizing mechanism – either assuming a small foot of fluid in front of the apparent contact line (precursor film, see [12,13,22]), or relaxing the no-

slip boundary condition at fluid–solid interface (see e.g., [23–26]). An earlier work [27] concentrated on these issues. In that paper it is shown that the results are rather insensitive to the choice of model (precursor versus slip), consistently with, e.g., [22]. However, the computational performance of the precursor film model is shown to be much better than that of various slip models. For this reason, here we also use a precursor film of thickness b (scaled by h_c) as a regularizing method.

The computational domain is chosen as a rectangle defined by $0 \le x \le L_x$ and $0 \le y \le L_y$ which is divided into $N_x \times N_y$ cells centered at node points (x_i, y_j) with $i = 1, \ldots, N_x$ and $j = 1, \ldots, N_y$. Eq. (3) is then discretized in space using a central finite difference scheme. The boundary conditions are chosen to model constant fluid flux far behind the fluid front. That is, we assume that there is an infinite stream of fluid far behind the front, that keeps the fluid height constant there. Within our nondimensionalization scheme, this leads to $h(0, y, t) = 1$ (see [28] regarding the issues related to constant volume configuration). We require that far ahead of the moving front, the fluid height is equal to the precursor thickness, $h(L_x, y, t) = b$, and also that the streamwise gradients of the fluid height vanish at the boundaries, i.e., $h_x(0, y, t) = h_x(L_x, y, t) = 0$. At the boundaries $y = 0$ and $y = L_y$, it is convenient to use $h_y(x, 0, t) = h_y(x, L_y, t) = 0$, $h_{yyy}(x, 0, t) = h_{yyy}(x, L_y, t) = 0$. This choice enforces no-flow across these boundaries. Time discretization is performed using implicit Crank-Nicolson scheme. We note that all the results presented in this paper are fully converged, as verified by grid refinement; more details about numerical issues can be found in [21].

3. Main features of the flow

Linear stability analysis (LSA) [12,13,22] of the governing Eq. (3) has shown that the flow is unstable with respect to fluid front perturbations in the transverse direction. LSA is performed by expanding to the first order all nonlinear terms in Eq. (3) about the base state. This base state is obtained as the y independent solution of Eq. (3) in a reference frame moving with velocity $c_0 = 1 + b + b^2$ [12].

The main results of LSA are illustrated in Fig. 2. These results are obtained by solving an eigenvalue problem of the form: $Lg(\xi) = \sigma g(\xi)$, where L is a linear operator, whose coefficients depend on the base solution $h_0(\xi)$ and $\xi = x - c_0 t$ [18]. We solve this problem and obtain the growth rate σ as the maximum value of the discretized spectrum. These calculations are performed using the routine real general generalized (RGG) from EISPACK for q's in the range $0 \le q \le 1.2$.

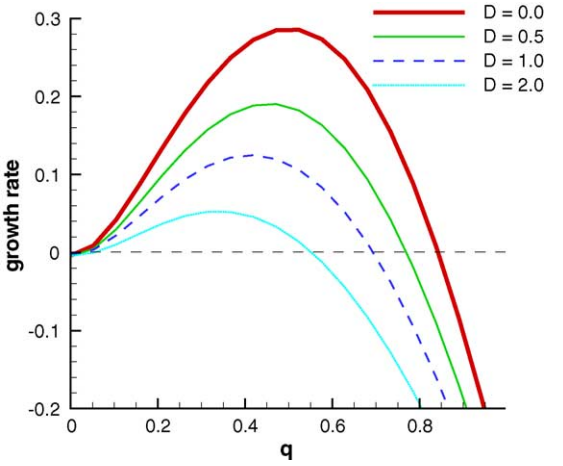

Fig. 2. Growth rate vs. wave number for few different values of D.

We see that the long wavelengths are unstable, while the short ones are stabilized by surface tension, represented by the fourth order term in Eq. (3). Consequently, there is a band of unstable modes bounded by the wavenumbers $q = 0$ and $q_c = 2\pi/\lambda_c$, where $\lambda_c \approx 8$ for $D = 0$, and $\lambda_c \approx 9$ for $D = 1$. The wavelength of maximum growth is approximately $\lambda^* = 2\pi/q^* \approx 12$–14, and it grows as the inclination angle is decreased, or, equivalently, as the parameter D in Eq. (3) is increased. At the same time, the growth rate of instability decreases as D is increased. We note that the importance of LSA is not only in explaining the early stage of instability. Although LSA is formally valid for short times only, one expects that the distance between resulting patterns in actual experiments is close to $\lambda_{\max}$ [28].

Figs. 3 and 4 show examples of our fully nonlinear simulations of the flow down a vertical plane, where $D = 0$, and an inclined one, where $D = 1$ (see [16,17]). These results show the development of instability in the nonlinear regime. Here, the initial condition is formulated by perturbing the straight contact line of the

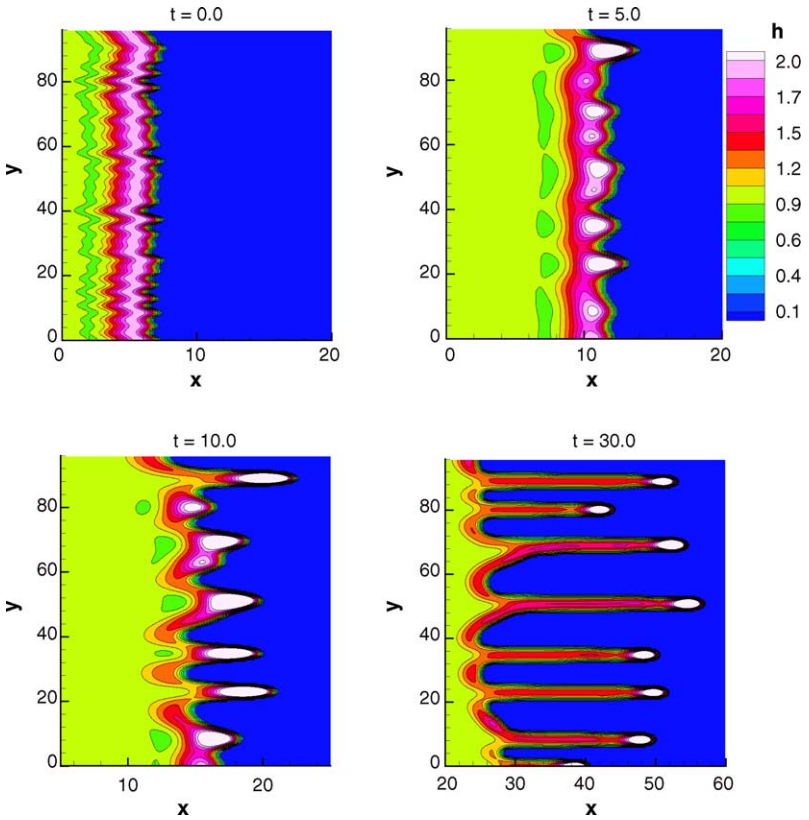

Fig. 3. Contour plot of the flow down an inclined plane ($D = 0$ and $b = 0.01$). At $t = 0$, contact line is perturbed by a superposition of 50 modes which were assigned random amplitudes.

base state with a superposition of $N = 50$ modes characterized by wavelengths $\lambda_{0,i} = 2L_y/i, i = 1, \ldots, 50$. Each mode is assigned a random length, L_0, in the range $[-0.2, 0.2]$.

Fig. 3 ($D = 0$) shows formation of long finger-like patterns. An average distance between these fingers is close to 12, in agreement with LSA. In Fig. 4 ($D = 1$), we see formation of triangular patterns, whose average distance is now about 16, again in agreement with linear stability.

Another feature is prominent in Fig. 4: the pattern length does not increase for late times – saturation is reached. We call these saturated patterns nontrivial traveling waves, so to distinguish from trivial, y-independent waves. For $D = 0$, however, these patterns are never reached in our simulations – not even for very long times, as discussed in the next section. This implies the existence of a critical D_{crit} below which a nontrivial traveling wave solution does not occur for the q's close to q^*. Whether this $D_{\text{crit}} = 0$ or not is an open question.

4. Growth saturation and nontrivial traveling waves

The growth saturation can be analyzed easier in the narrow computational domains where only a single pattern (finger or a triangle) is present; therefore, nonlinear mode interaction is avoided. Fig. 5 shows the snapshots of fluid fronts for $D = 0$ and $D = 1$. Here, we see even more clearly a significant difference between these two cases. For $D = 0$ the length of the pattern grow for all times, while for $D = 1$ the grow slows down and then eventually stops, similarly as in the large domain case of Fig. 4.

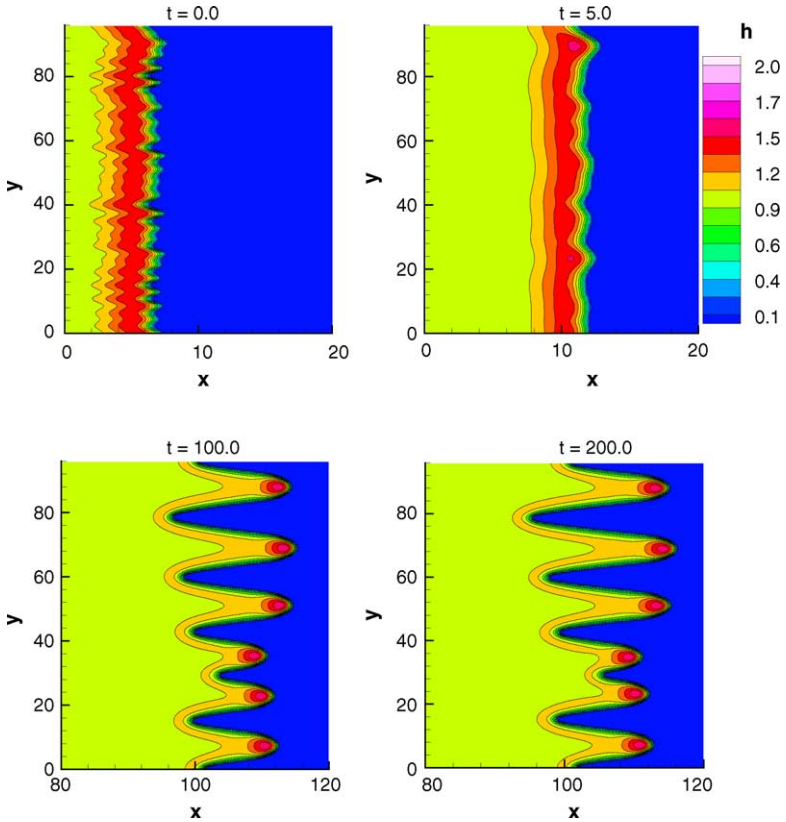

Fig. 4. Contour plot of the flow down an inclined plane ($D = 1$ and $b = 0.01$). At $t = 0$, contact line is perturbed by a superposition of 50 modes which were assigned random amplitudes.

Fig. 6 shows pattern length as a function of time for a set of D's. The growth saturates at smaller pattern lengths for larger D's, as one would expect, since an increase of D reduces the instability. For $D = 0$, as pointed out above, the growth does not saturate. We note that the lack of saturation for $D = 0$ case is not there simply because we have not waited for sufficiently long time: We have performed simulations up to time $t = 1000$ – at that time, $L/L_0 \approx 4000$, without any sign of saturation!

The question of whether $D = 0$ is a singular limit is an interesting one. Careful experimental results which could answer this question, to our best knowledge, do not yet exist. An additional complication regarding experiments is that most of them are performed using fixed amount of fluid; the resulting change of the base fluid height modifies the problem significantly. Computational results for this problem are also limited and include only a couple of works [14,16], which we discuss next.

Our earlier work [16] showed that there are two parameters which have a strong influence on the pattern growth of the $D = 0$ case: (i) size of the computational domain in the transverse, y, direction, and (ii) precursor film thickness.

The precursor film (or, similarly, slipping length [27]), are, essentially, regularizing parameters. For computational efficiency, these quantities are typically much larger in computations than in real physical systems [28]. Clear, it is important to verify whether if these quantities are given large values, there is no change in the qualitative features of the computed results. Indeed, in [17] we have shown that that this is a serious concern, since by using large values of b we were able to reduce the growth rate even for $D = 0$ case. However, as long as b is less than about 0.01, the

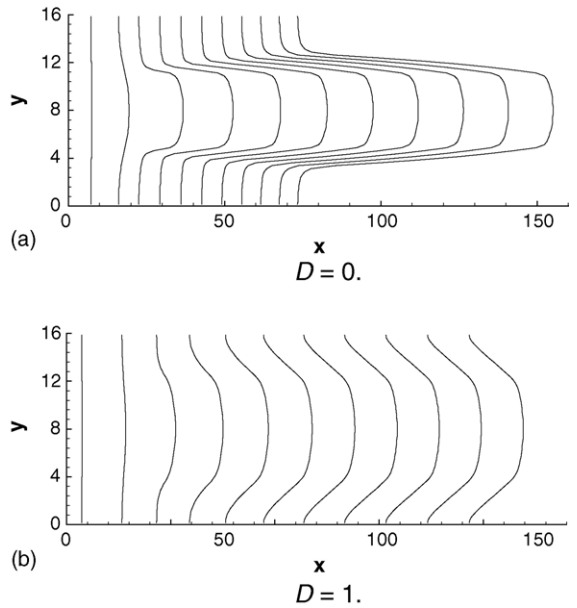

Fig. 5. Snapshots of the patterns in $\delta t = 20$ intervals. Note continuously increasing length for $D = 0$ and length saturation for $D = 1$.

important features of the flow do not depend on b. In this work, we therefore fix $b = 0.01$, and concentrate on the second important parameter that influences the growth.

Fig. 7 shows the influence of the size of the computational domain on the flow down a vertical plane ($D = 0$). We see that if the computational domain is sufficiently narrow, for long times one does observe

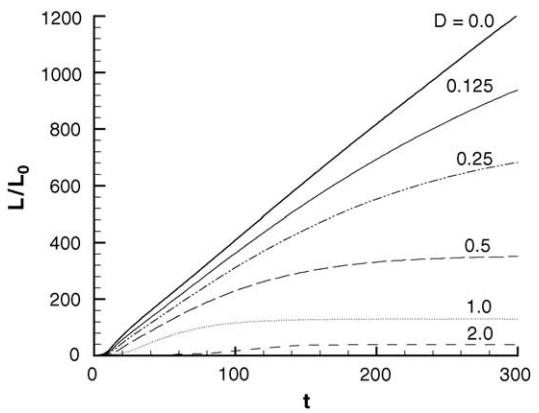

Fig. 6. Length of the emerging patterns for different D's.

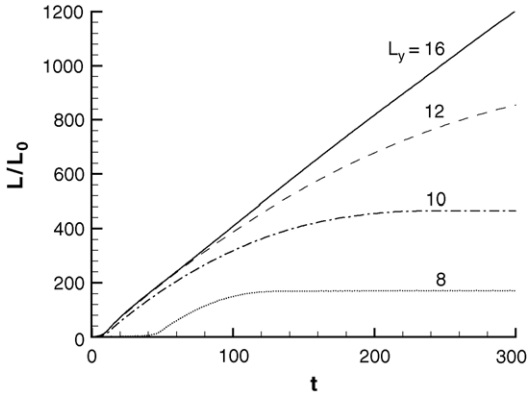

Fig. 7. Length of the emerging patterns for $D = 0$ and for different L_y's.

growth saturation. This result is consistent with the earlier results [14], which reported growth saturation for $D = 0$ in narrow computational domains. [However, the influence of the domain size on the growth saturation was not discussed in [14]].

This domain size dependence seems to be a sign that an interesting new insight can be gained by analyzing in more detail the behavior of the system close to the critical wavenumber, q_c. Computational analysis of this behavior is the subject of the next section.

5. Bifurcation analysis close to the critical wavenumber

To explore the behavior close to q_c, we perform a set of simulations of the flow perturbed by a given wavenumber q, in a domain of width $L_y = 2\pi/q$. We then vary the size, L_0, of applied perturbation at $t = 0$, as well as q itself, and follow the instability development for long times. Since the flow is simpler in the case $D > D_{\text{crit}}$, we concentrate first on this configuration.

Fig. 8a shows the results close to q_c for $D = 1$. For $q > q_c$, and if the initial length of the perturbation is sufficiently small (presented by the hollow circles in the figure), the system relaxes to the trivial (y-independent) state. However, if the initial amplitude is increased (the hollow squares in the figure), the system jumps to another stable state: These are nontrivial

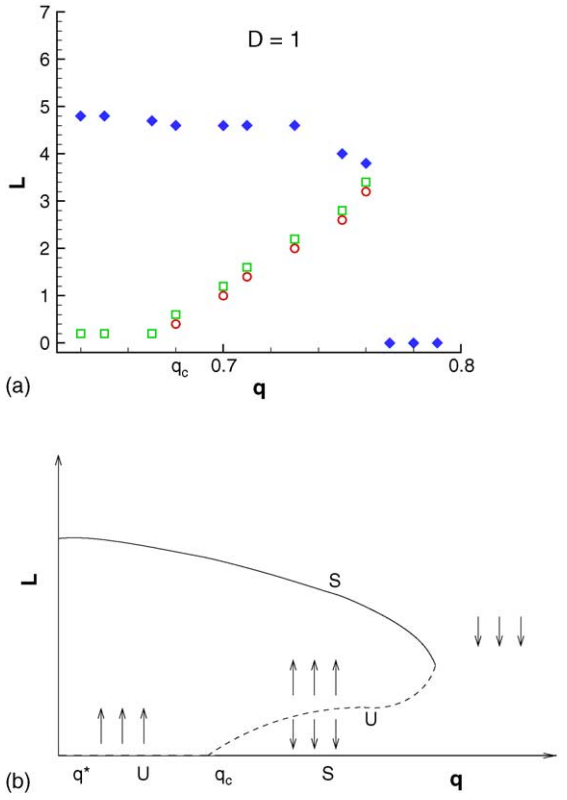

Fig. 8. Bifurcation diagram for the flow down an inclined plane for $D > D_{\text{crit}}$, showing the steady pattern length, L, vs. the wave number, q. (a) Numerical results: largest initial lengths, L_0's, that converge to the trivial state (hollow circles), smallest L_0's that converge to a nontrivial steady state (hollow squares), and the final length of the patterns (filled diamonds). (b) Bifurcation sketch: stable (S) and unstable (U) branches.

traveling waves. These profiles, or more precisely their final (saturated) length, are represented by the filled symbols in the figure. The final length is almost independent of q, although it is slightly smaller for very large q's. These nontrivial waves occur only for q's that are small enough: If q is sufficiently large (more than about 0.76 for this particular D), any perturbation converges to the trivial state. Finite length waves exist for all smaller q's. This property has already being exemplified earlier in Figs. 4, 5b, and 6.

Fig. 8b sketches the possible bifurcation diagram. In this figure, the arrows point in the direction of the increase or decrease of the patterns' lengths. Our results show that the nontrivial stable branch keeps propagating towards smaller and smaller q's, in the manner reminiscent of the subcritical bifurcation of hexagonal cells from the trivial state in Rayleigh–Bernard convection [29].

To conclude the discussion of $D > D_{\text{crit}}$ case, we note that the final length of the patterns does not depend on the initial L_0, as long as L_0 is large enough; this point is discussed in more detail below. Additional results (not given here) show that as D is increased, the slope of the stable nontrivial branch decreases as well, consistently with the results shown in Fig. 6.

Fig. 9a shows the corresponding results for $D = 0$. Here, we see a similar bifurcation structure as for $D = 1$ in the immediate vicinity of q_c (note that q_c here is different from the one for $D = 1$). The main difference of the results compared to $D = 1$ is that here we obtain nontrivial traveling waves only in a given range of q's. If q is sufficiently large (more than about 0.93), any initial perturbation decays to a trivial state, similarly to $D = 1$. However, if q is sufficiently small, the saturation does not occur for any initial perturbation, and nontrivial traveling waves cease to exist. An obvious possibility, sketched in Fig. 9b, is that the nontrivial stable branch does not continue towards smaller q's, as it did for $D = 1$, but instead it turns over at some value of $q = q_1$, which lies between q^* and q_c. For $q < q_1$, any initial perturbation leads to unstable state that, according to our simulations, grows without limit.

Next we outline some features of the flow which are important for better understanding of the traveling waves, and of the differences between $D < D_{\text{crit}}$ and $D > D_{\text{crit}}$. In particular, we discuss the influence of the initial perturbation, and of the wavenumber q on the final configuration, again first for $D = 1$ and then for $D = 0$.

First, we verify that the final pattern length, L, does not depend on the initial perturbation, L_0. Fig. 10 shows that this is indeed the case. In this figure we plot the pattern length for $D = 1$, $L_y = 9.4$ (corresponding to $q = 0.67$) and for few different L_0's. We see that the initial length of the perturbation modifies not only the time needed for the pattern to grow to its final length L, but also L itself. Interestingly, we also observe an 'overshoot' in the pattern length. This novel feature of the flow is present for all flows down an incline for which $D > D_{\text{crit}}$.

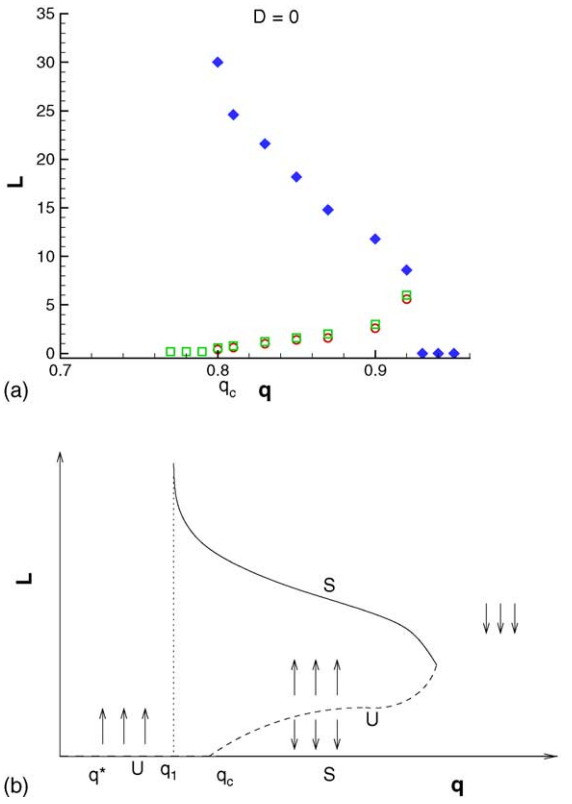

Fig. 9. Bifurcation diagram for the flow down an inclined plane for $D = 0$. (a) Numerical results: largest initial perturbation lengths, L_0's that converge to the trivial state (hollow circles), smallest L_0's that converge to a nontrivial steady state (hollow squares), and the final length of the patterns (filled diamonds). (b) Bifurcation sketch: stable (S) and unstable (U) branches.

Second, we discuss the pattern growth in the case where the initial perturbation is kept fixed, but q varies. Fig. 11 shows that the maximum finger length (the 'overshoot') does depend (although rather weakly) on q. For smaller q's (larger L_y's), we observe larger maximum length. However, the final saturated length is almost constant for all q, as it can be already seen in Fig. 8a.

For $D = 0$, we obtain very different results. Fig. 12 shows the resulting pattern length for the largest q that still leads to formation of (nontrivial) traveling waves. The final pattern length does not depend on the initial perturbation L_0, similarly as for $D = 1$. However, there is a difference compared to $D = 1$, and that is that there is no 'overshoot' here. The final pattern length is reached rather early in the flow evolution (slightly

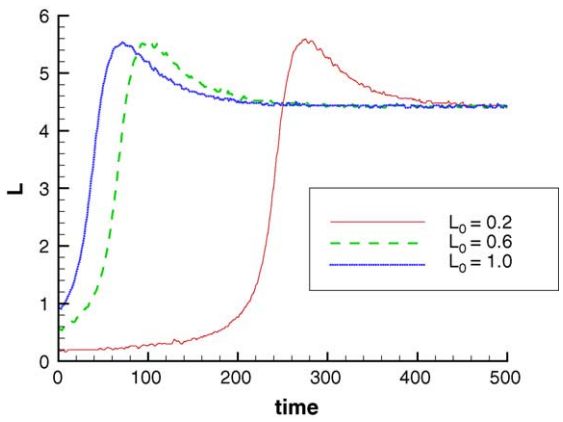

Fig. 10. Pattern length for $D = 1$ and $L_y = 9.4$, corresponding to $q \approx 0.67$. Small oscillations are related to grid-size effects.

faster in the case of larger L_0) and then this length persists for all explored times. We conjecture that the difference between $D < D_{\text{crit}}$ and $D > D_{\text{crit}}$ flows is not only the existence (or lack of it) of nontrivial traveling waves, but also the manner in which the patterns form for $q \approx q_c$. More research is needed to fully understand this problem.

6. Future work

In this paper we present the main ideas and numerical evidence regarding the nature of the bifurcation close to the critical wavenumber. While these numer-

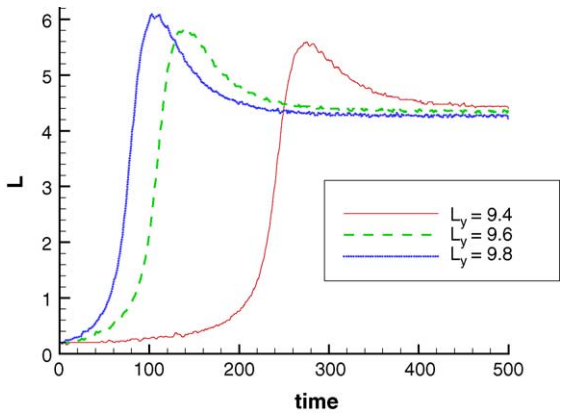

Fig. 11. Pattern length for $D = 1$ and for $L_0 = 0.2$, for $L_y = 9.4$, 9.6, and 9.8, corresponding to $q \approx 0.67$, 0.655, and 0.64, respectively.

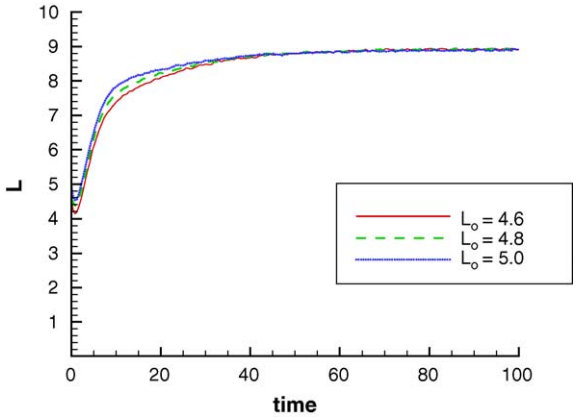

Fig. 12. Pattern length for $D = 0$ and $L_y = 6.8$, corresponding to $q \approx 0.92$.

ical results already provide significant insight into the problem, we expect that more precise understanding can be reached via regular perturbation analysis. Although we do not present the results here, we outline the main steps.

Assume that at $t = 0$ there is a single mode present, characterized by an initial length L_0 and the wavenumber q. Next, rescale Eq. (3) by defining $\zeta = qy/(2\pi)$, so that q appears explicitly in the equation. Consider the problem in the reference frame moving with speed c_0, and recall $\xi = x - c_0 t$. Then, expand Eq. (3) in terms of small parameter ϵ around the bifurcation point $q = q_c$ as

$$\begin{aligned} &q = q_c + \epsilon\bar{q} + \ldots, \\ &h(\xi, \zeta, t) = h_0(\xi) + \epsilon\bar{h}(\xi, \zeta, t) + \ldots, \\ &\tau = \sigma(\epsilon)t, \\ &\sigma(\epsilon) = \epsilon\bar{\sigma} + \ldots, \end{aligned} \tag{4}$$

where the leading order term in the expansion of σ is absent in the moving frame [30,31]. It is worth pointing out that the base state, h_0, about which one expands, is given as a solution of the following nonlinear ODE

$$-c_0 h_0 + h_0^3 h_{0\eta\eta\eta} - D(\alpha) h_0^3 h_{0\eta} + h_0^3 = d, \tag{5}$$

and is hence known only numerically (d and c_0 are the constants related to the boundary conditions; for precursor model used here, $d = -b(b+1)$, and $c_0 = 1 + b + b^2$). Therefore, the asymptotic analysis will lead to a series of (linear) problems for the corrections which will have to be solved numerically as well. The results of this analysis should then be compared to the numerical results presented here. This approach should provide an answer to the question whether D_{crit} vanishes or not. The result that $D_{\text{crit}} = 0$ would be very interesting, since it would imply that the nature of the solutions of Eq. (3) depends in a singular way on D, i.e., Eq. (3) would be structurally unstable.

Acknowledgements

We thank Burt Tilley for useful comments. L. K. acknowledges support from NSF grant No. INT-0122911 and J. D. support from Consejo Nacional de Investigaciones Científicas y Técnicas, CONICET-Argentina.

References

[1] S.J. Weinstein, K.J. Ruschak, Coating flows, Annu. Rev. Fluid. Mech. 36 (2004) 29.
[2] M.A. Spaid, G.M. Homsy, Viscoelastic free surface flows: spin coating and dynamic contact lines, J. Non-Newtonian Fluid. Mech. 55 (1994) 249.
[3] S.K. Wilson, R. Hunt, B.R. Duffy, The rate of spreading in spin coating, J. Fluid. Mech. 413 (2000) 65.
[4] K.B. Glasner, T.P. Witelski, Coarsening dynamics of dewetting films, Phys. Rev. E 67 (2003) 016302.
[5] U. Thiele, K. Neuffer, M. Beshehorn, Y. Pomeau, M.G. Velarde, Sliding drops on an inclined plane, Colloid. Surf. A 206 (2002) 87.
[6] L.M. Pismen, Y. Pomeau, Disjoining potential and spreading of thin liquid layers in the diffuse-interface model coupled to hydrodynamics, Phys. Rev. E 62 (2000) 2480.
[7] S.M. Troian, Stabilizing the advancing front of thermally driven climbing films, Nature 203 (1998) 335.
[8] L. Kondic, J. Diez, Flow of thin films on patterned surfaces: Controlling the instability, Phys. Rev. E 65 (2002) 045301.
[9] M.R.E. Warner, R.V. Craster, O.K. Matar, Dewetting of ultra-thin surfactant-covered films, Phys. Fluids 14 (2002) 4040.
[10] J. Sur, A.L. Bertozzi, R.P. Behringer, Reverse undercompressive shock structures in driven thin film flow, Phys. Rev. Lett. 90 (2003) 126105.
[11] E.B. Dussan V, On the spreading of liquids on solid surfaces: Static and dynamic contact lines, Annu. Rev. Fluid Mech. 11 (1979) 317.
[12] S.M. Troian, E. Herbolzheimer, S.A. Safran, J.F. Joanny, Fingering instabilities of driven spreading films, Europhys. Lett. 10 (1989) 25.
[13] A.L. Bertozzi, M.P. Brenner, Linear stability and transient growth in driven contact lines, Phys. Fluids 9 (1997) 530.
[14] M.H. Eres, L.W. Schwartz, R.V. Roy, Fingering phenomena for driven coating films, Phys. Fluids 12 (2000) 1278.

[15] D.T. Moyle, M.S. Chen, G.M. Homsy, Nonlinear rivulet dynamics during unstable dynamic wetting flows, Int. J. Mult. Flow 25 (1999) 1243.
[16] J. Diez, L. Kondic, Contact line instabilites of thin liquid films, Phys. Rev. Lett. 86 (2001) 632.
[17] L. Kondic, J. Diez, Contact line instabilities of thin film flows: Constant flux configuration, Phys. Fluids 13 (2001) 3168.
[18] Y. Ye, H. Chang, A spectral theory for fingering on a prewetted plane, Phys. Fluids 11 (1999) 2494.
[19] J.M. Davis, S.M. Troian, On a generalized approach to the linear stability of spatially nonuniform thin film flows, Phys. Fluids 15 (2003) 1344.
[20] R.O. Grigoriev, Contact line instability and pattern selection in thermally driven liquid films, Phys. Fluids 15 (2003) 1363.
[21] J. Diez, L. Kondic, Computing three-dimensinal thin film flows including contact lines, J. Comp. Phys. 183 (2002) 274.
[22] M.A. Spaid, G.M. Homsy, Stability of Newtonian and viscoelastic dynamic contact lines, Phys. Fluids 8 (1996) 460.
[23] H.P. Greenspan, On the motion of a small viscous droplet that wets a surface, J. Fluid Mech. 84 (1978) 125.
[24] E.B. Dussan V, The moving contact line: the slip boundary condition, J. Fluid Mech. 77 (1976) 665.
[25] L.M. Hocking, A.D. Rivers, The spreading of a drop by capillary action, J. Fluid. Mech. 121 (1982) 425.
[26] E.O. Tuck, L.W. Schwartz, A numerical and asymptotic study of some third-order ordinary differential equations relevant to draining and coating flows, SIAM Rev. 32 (1990) 453.
[27] J. Diez, L. Kondic, A.L. Bertozzi, Global models for moving contact lines, Phys. Rev. E 63 (2001) 011208.
[28] J. Diez, A.G. González, J. Gomba, R. Gratton, L. Kondic, Unstable spreading of a fluid filament on a vertical plane: Experiments and simulations, Physica D (2004) (this volume).
[29] P.G. Drazin, W.H. Reid, Hydrodynamic Stability, Cambridge University Press, Cambridge, 1991.
[30] B.S. Tilley, S.H. Davis, S.G. Bankoff, Nonlinear long-wave stability of superposed fluids in an inclined channel, J. Fluid. Mech. 277 (1994) 55.
[31] M.C. Cross, P.C. Hohenberg, Pattern formation outside of equilibrium, Rev. Mod. Phys. 65 (1993) 851.